Electronic Supplementary Information

Metallic Co_2P Ultrathin Nanowires Distinguished From CoP as Robust Electrocatalysts for Overall Water-Splitting

*Zhaoyu Jin, Panpan Li and Dan Xiao**

Experimental Section

Synthesis of Co_2P NWs. The CPNWs were prepared according to a facile decomposition of Co - tri-n-octylphosphine method but with some modifications.[1-3] A mixture of 1.5 mmol cobalt (II) acetylacetonate (Sigma-Aldrich), 4.5 mmol oleic acid (Aladdin) and 5-mL trioctylphosphine (Alfa Aesar) was heated to 120 ℃ under magnetic stirring with nitrogen protecting in Schlenk line. After complete removal of water via vacuum-nitrogen cycles in the mixed solution, the precursor was sealed into a thick-walled pressure flask and rapidly microwave-heated for ~ 15 min (700 W output power) at above 350 ℃. The black precipitate was produced in the bottom then centrifuged and washed by ethanol and hexane for three times after cooled to the room-temperature. Afterwards, the surfactant on the cobalt phosphide was removed by annealing at 400 ℃ under the protection of nitrogen/hydrogen. The sample was finally dried in the vacuum at ~ 60 ℃ overnight. As for the bulk Co-P film, a smooth pure cobalt foil was used as the cobalt source and the other condition and method were the same as the preparation of Co_2P NWs.

Synthesis of CoP NWs. The method to obtain CoP nanowires was followed the reference[2] and described briefly below: Firstly, 1.5 mmol cobalt (II) acetylacetonate (Sigma-Aldrich), 4.5 mmol oleic acid (Aladdin) and 5-mL trioctylphosphine (Alfa Aesar) were added to a 50 mL Schlenk flask. Then the mixture was heated to 100 ℃ and pumped the water by the vacuum. Afterwards, the temperature was increased to 380 ℃ under nitrogen gas with a rate of 10 ℃ min^{-1}. As soon as the black powder generated from the violet solution, we maintained the temperature for ~2 h until the Co_2P was fully transfer to CoP. Finally, the product was centrifuged by ethanol and hexane for three times and the surfactant was removed through the above annealing method.

Characterizations. Scanning electron microscopy (SEM) analysis was carried out on a field emission Hitachi S4800 microscope (Japan). The energy-dispersive X-ray analysis (EDX) was determined by a EDAX detector (USA). The high-resolution transmission electron microscopy (HRTEM) images were recorded by a FEI Tecnai G2 F20 S (USA) with an accelerating voltage of 200 kV. X-ray diffraction (XRD) analysis was performed on a Fangyuan DX-1000 powder X-ray diffractometer (China) with Cu Ka radiation at 40 kV. X-ray photoelectron spectra (XPS) were acquired with Kratos AXIS ULTRA DLD Photoelectron Spectroscope (UK) with element carbon as internal standard.

Electrochemical measurements. Catalyst inks for electrochemical testing were prepared by adding 2 mg catalyst powders to a mixture of 500 μL distilled water / isopropyl alcohol (3:1, v/v) and 10μL Nafion solution (5% wt, Dupont, USA). After ultrasonical dispersion to homogeneous, 2μL fresh catalyst ink were cast onto a glassy carbon (GC) with a mass loading of 170 μg cm^{-2} and dried at the room-temperature. All electrochemical tests were carried out on a computer-controlled Autolab PGSTAT 12 potentiostat / galvanostat (Metrohm, Switzerland) in 0.5 M H_2SO_4 or 1.0 M KOH with Ag/AgCl as reference electrode and platinum foil as counter electrode. The data were calibrated to the reversible hydrogen electrode (RHE) obtained from the calibration equation: E (RHE) = - 0.059 × pH + 0.197 + E(Ag/AgCl) - iR. The iR drop of all polarization curves was determined by the equivalent circuits fitted from the electrochemical impedance spectra (EIS), which give the solution resistance of 1.5 ohm and 1.2 ohm for 1.0 M KOH and 0.5 M H_2SO_4, respectively. The linear sweep voltametric (LSV) curves were obtained by sweeping the potential at a low scan rate of 5 mV s^{-1}, while the solution was stirred with a magnetic stir bar. Cyclic voltametric (CV) curves were controlled the scan rate at 20 mV s^{-1}. Moreover, regarding the alkaline water electrolysis with the two-electrode configuration, the catalyst inks were prepared by adding 8 mg catalyst powders to a mixture of 1 mg acetylene black and 1 mg polyvinylidene fluoride. After dissolved and grinded completely into a homogeneous state, the inks were then dropped on a clean nickel foam with a mass loading of 2 mg cm^{-2}. The electrode was dried at the room-temperature for 3 hours and at 80 ℃ in the vacuum for 30 min before used.

Calculation of density of states (DOS). The density function theory (DFT) calculations were performed through the Cambridge serial total package (CASTEP).[4] The generalized-gradient approximation (GGA) in the Perdew−Burke−Ernzerhof (PBE) form with a cutoff for the plane waves of 340 eV was employed. We used 3 × 1 × 1 unit cells of Co_2P and CoP for geometric optimization. The k- points grid of 5 × 1 × 1 was used for calculating the densities of states and the thickness of vacuum space was set to be 15 Å.

Characterizations of the Co_2P and CoP nanowires:

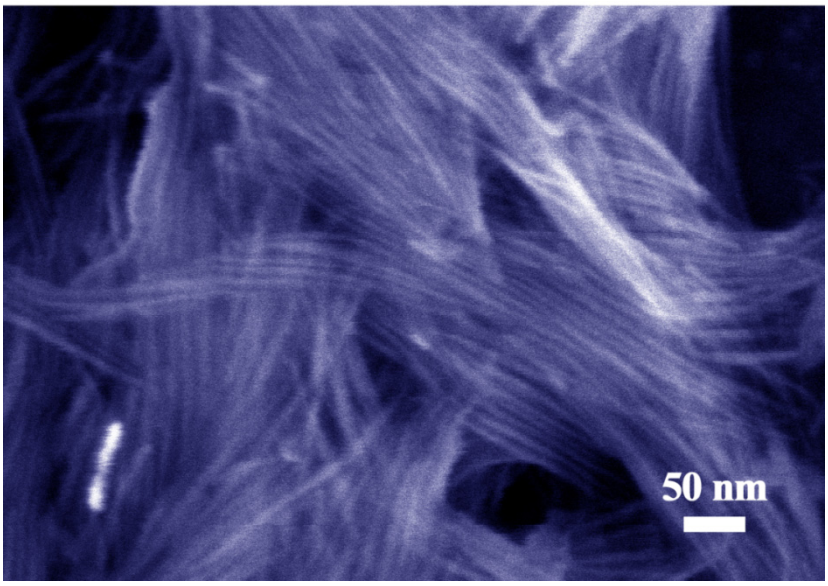

Fig. S1 SEM images of the Co_2P nanowires.

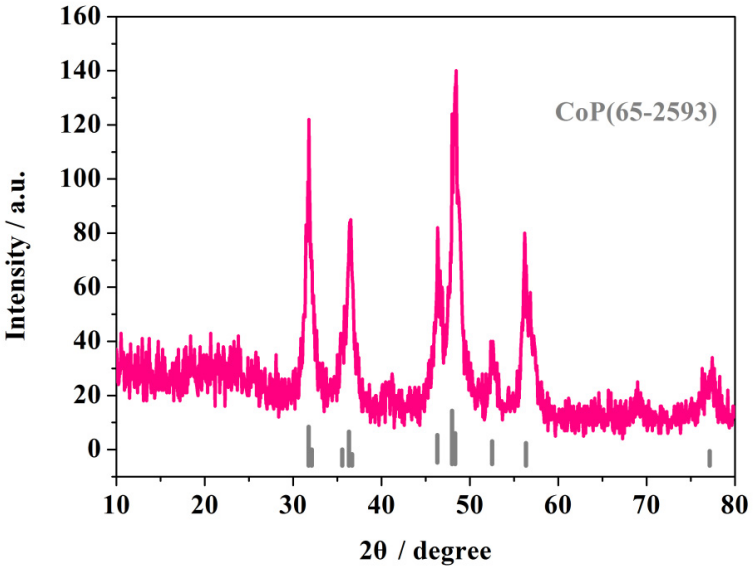

Fig. S2 XRD pattern of the as-synthesized CoP NWs.

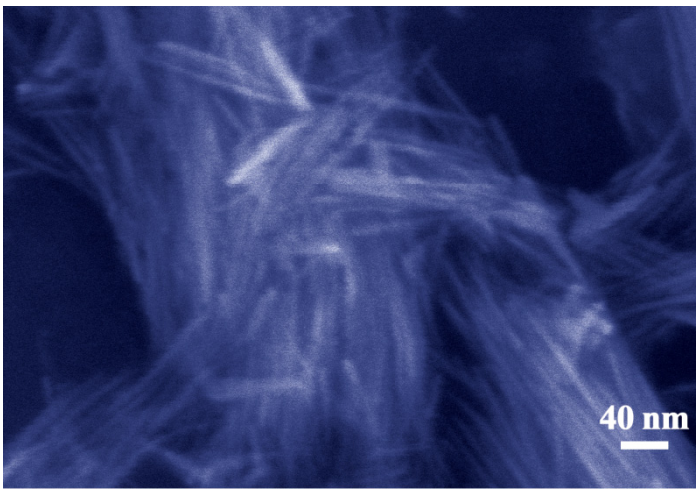

Fig. S3 SEM image of CoP nanowires.

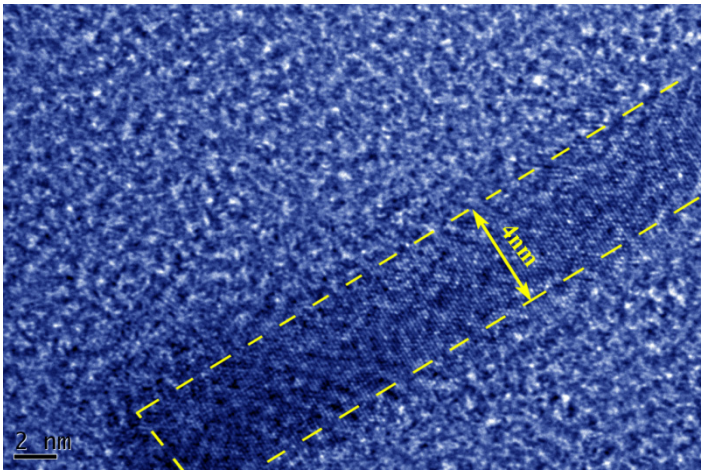

Fig. S4 HRTEM images of CoP nanowire.

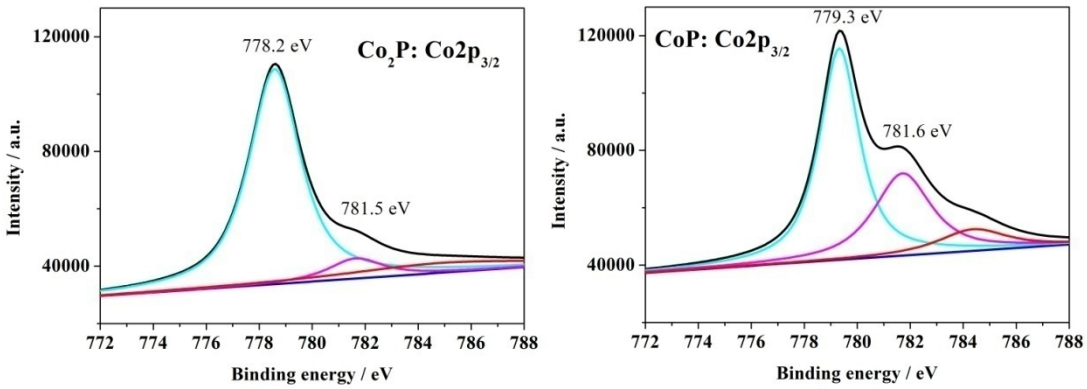

Fig. S5 the deconvoluted XPS spectra for Co $2p_{3/2}$ of Co_2P (left)and CoP (right).

Table S1 Charges of cobalt in different catalysts calculated by the method reported from the ref.5.

catalyst	**charges of Co**
CoP	+0.7
Co_2P	+0.3
bulk Co-P film	+2

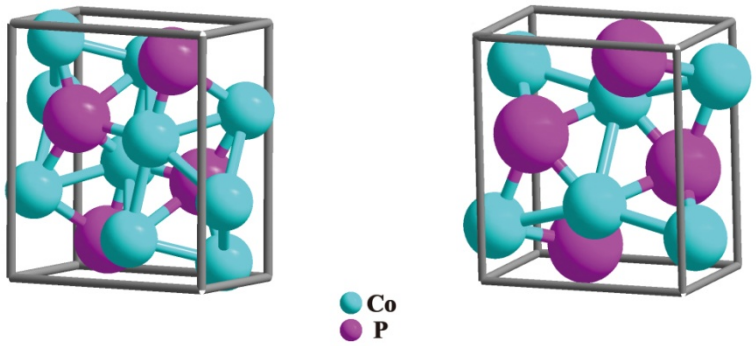

Fig. S6 The crystal structures of Co_2P **(left)** and CoP **(right)** described as ball-and-stick model. Cobalt atoms (blue) are much more in the Co_2P than phosphorous atoms (purple). Especially, many Co atoms occupy the positions at the edge and surface.

Elemental analysis:

Table S2 XRF survey of the Co_2P nanowires.

Element	Content (atomic) %
Co	36.509
P	18.532
O	44.959

Table S3 XRF survey of the CoP nanowires.

Element	Content (atomic) %
Co	29.584
P	28.831
O	41.585

As for the purity of the sample, we carried out the overall element analysis by XRF to determine the atomic ratio of Co / P. The results display: Co / P = 23.5 % / 12.0 % = 1.96 (Co_2P); Co / P = 19.6 % / 19.8 % = 0.99 (CoP). The XRF analysis demonstrates a near value of the stoichiometric ratio for both Co_2P and CoP, which indicates the sample we prepared is indeed the cobalt phosphide with little impurities. By the way, the powder sample was loaded on the FTO glass for the XRF testing, so the result shows high oxygen concentration in the sample.

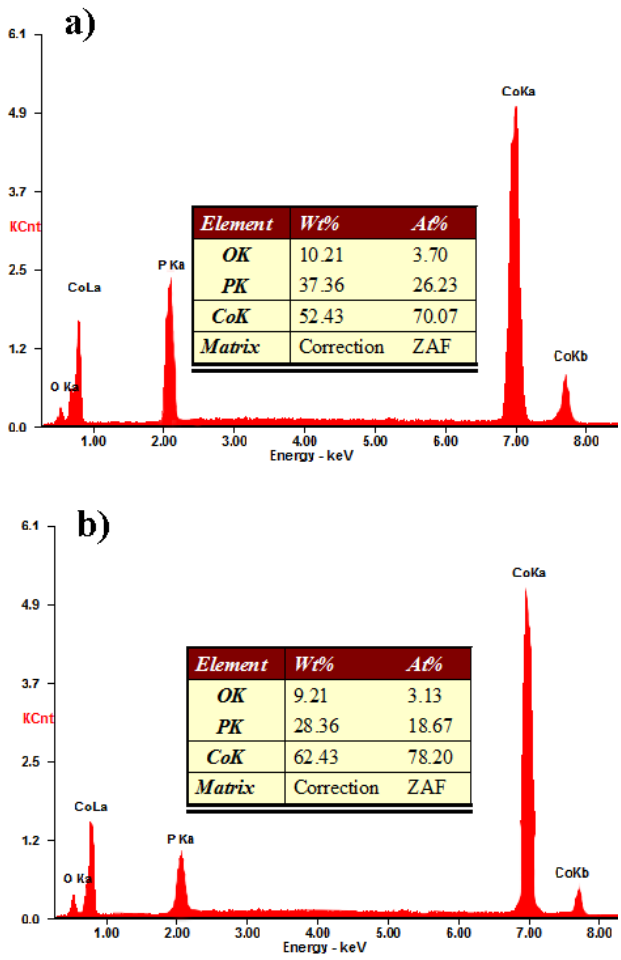

Fig. S7 EDX spectra and corresponding element compositions of the a) CoP NWs and b) Co_2P NWs.

The results reveal the phosphide degree of the two cobalt phosphide is different. The reason could be found from the formation mechanism of the TOP method. Firstly, the metal cation (Co^{2+}) was reduced to the metallic state (Co^0 cluster) by the oleic acid at ~ 300 ℃.[1] Afterwards, when the temperature was increased to ~380 ℃, the TOP which bound with the cobalt was decomposed as well as generated the cobalt phosphide from the surface to the inner. The head-product was Co_2P because of the lower phosphorous needed. While the reaction was continuous, the Co_2P would undergo the deep phosphide process together with TOP to form CoP.[6] Thus we could observe from the XRF and EDX results the CoP with higher phosphide degree than Co_2P.

Characterizations of bulk Co-P film:

We then carried out the characterizations of the bulk Co-P film directly grown on Co foil. From the XRD pattern in Fig. S8, the phases of film are identified as the CoP_4 and $Co_2P_2O_7$. XPS spectra of Co 2p and P 2p in Fig. S9 demonstrate the charged state of the Co-P film, which is apparently different from the Co_2P and CoP NWs. The peaks of Co 2p at 781.9 and 798.5 eV and the corresponding satellite peaks are assigned to the Co(II). And the peak of P 2p also reveals the presence of phosphate. Because XPS is a superficial analysis that usually captures the information near the surface of the material (5 ~ 10 nm), the cobalt phosphate is majorly formed on the surface. In addition, the EDX spectrum exhibits the elemental ratio of the bulk Co-P film on the cobalt foil.

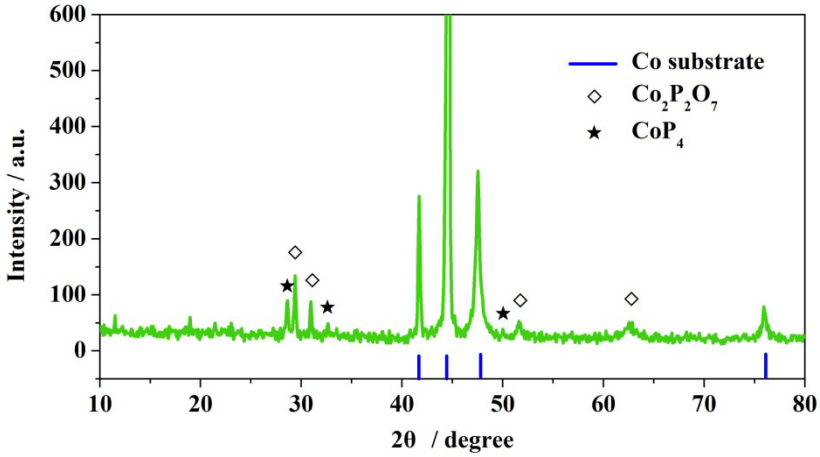

Fig. S8 XRD pattern of the bulk Co-P film directly grown on cobalt foil.

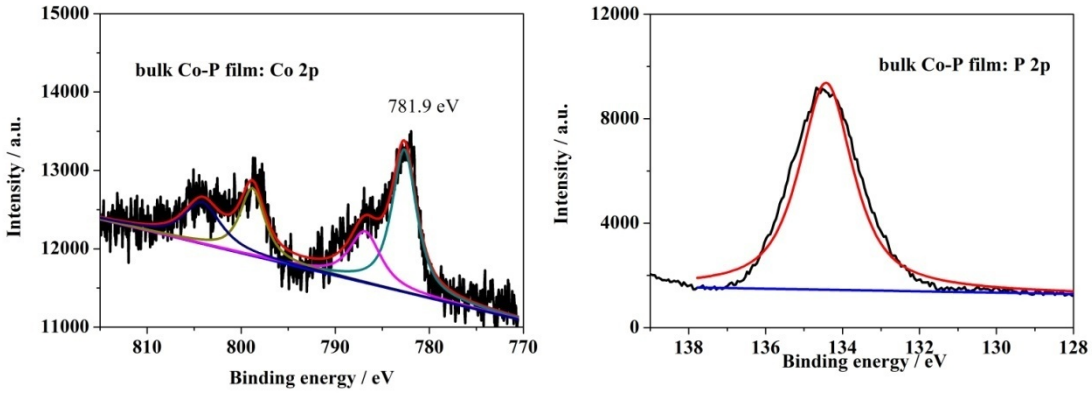

Fig. S9 XPS spectra of Co 2p (left) and P 2p (right).

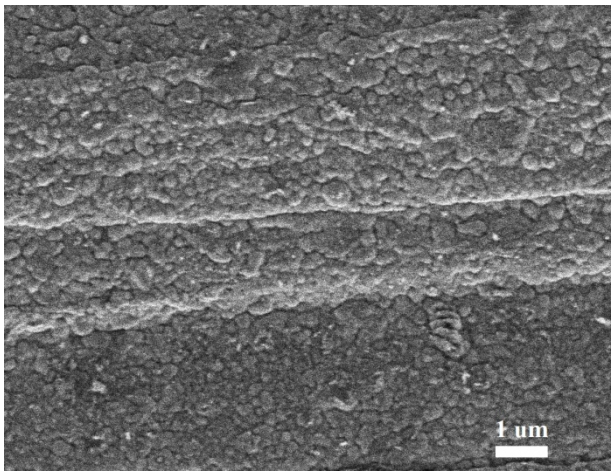

Fig. S10 SEM image of the bulk Co-P film.

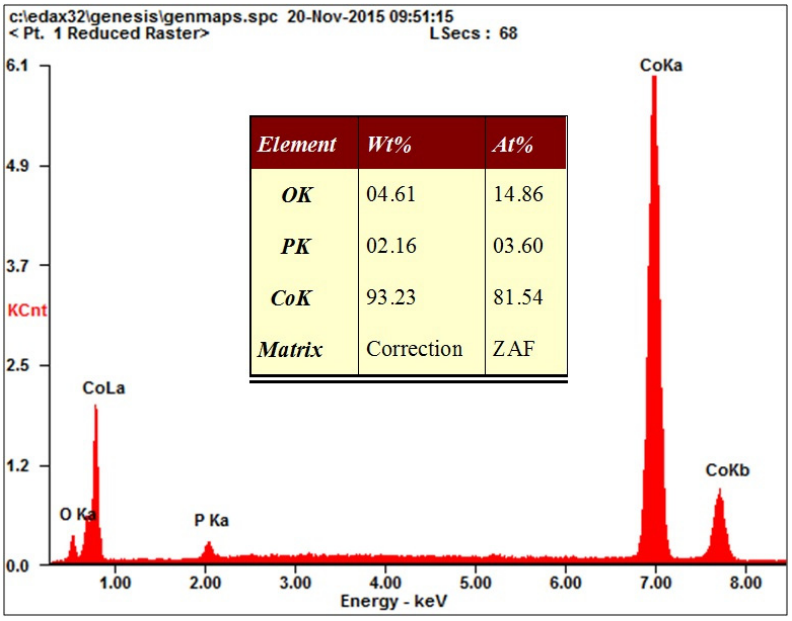

Fig. S11 EDX spectrum and element analysis of bulk Co-P film.

Additional electrochemical measurements:

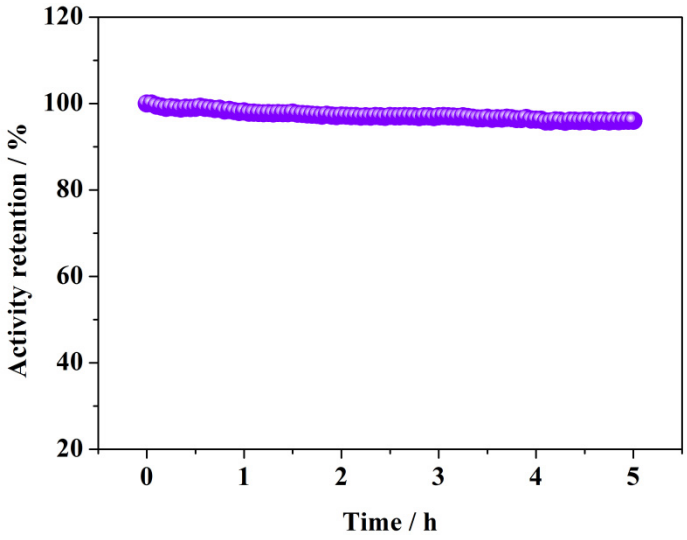

Fig. S12 The long-term stability of the Co_2P NWs for HER in 0.5 M H_2SO_4.

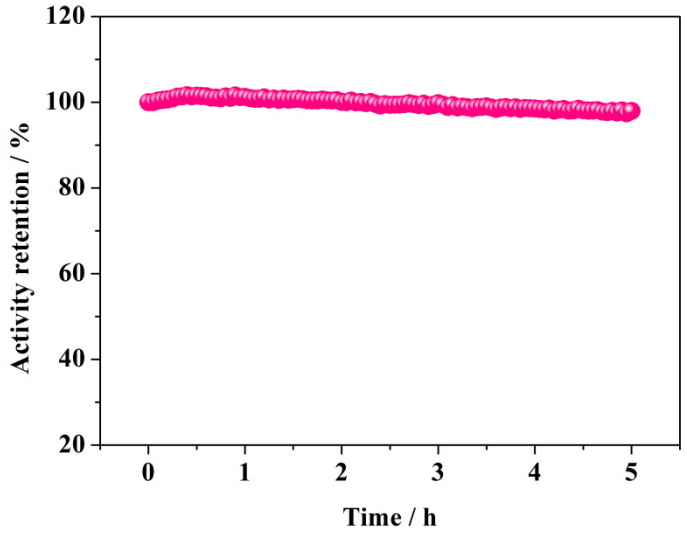

Fig. S13 The long-term stability of the Co_2P NWs for OER in 1 M KOH.

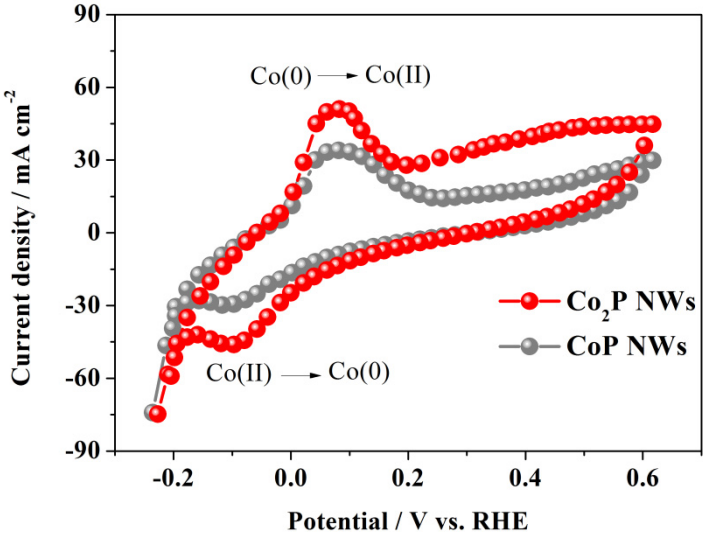

Fig. S14 CVs in 1 M KOH with a Ni foam as the catalyst loading.

A pair of redox peaks are corresponding the electrochemical reaction for the cobalt phosphide in both Co_2P and CoP.[7]

anodic peak: $Co_2P + 2OH^- \rightarrow Co(OH)_2 + Co + P + 2e^-$ (1^{st} cycle)

or $Co + 2OH^- \rightarrow Co(OH)_2 + 2e^-$

cathodic peak: $Co(OH)_2 + 2e^- \rightarrow Co + 2OH^-$

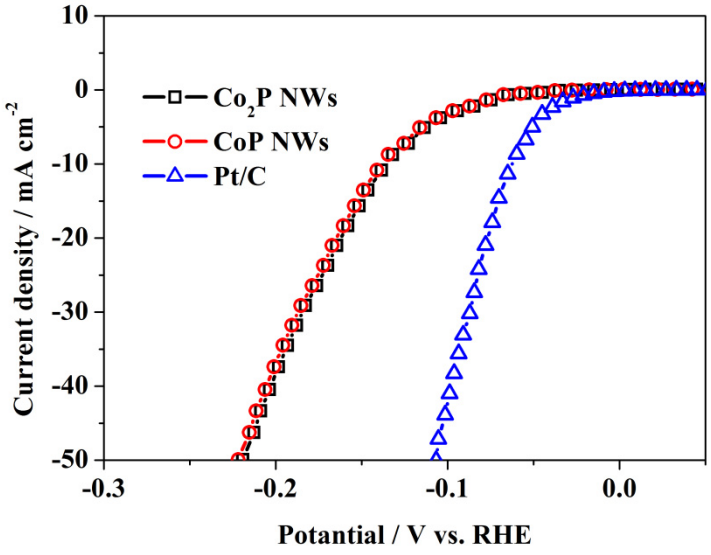

Fig. S15 Hydrogen evolution in 1 M KOH for the Co_2P NWs, CoP NWs and Pt/C.

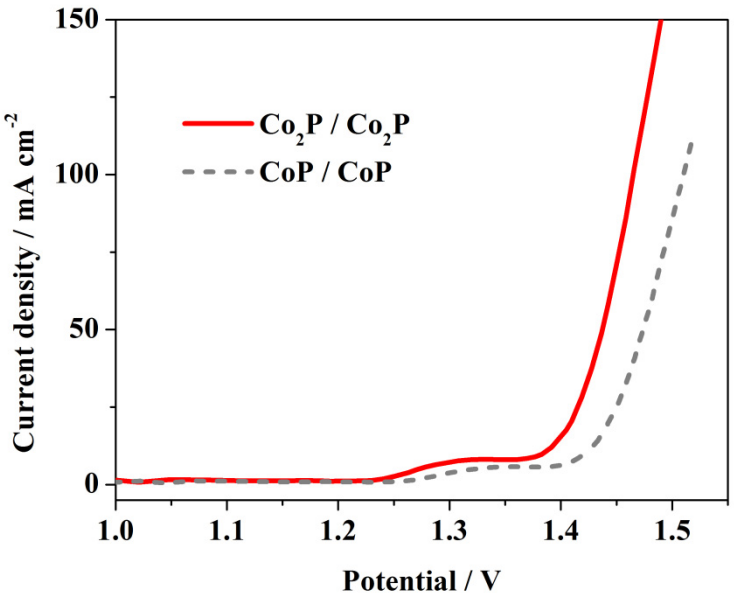

Fig. S16 Polarization curves of the two-electrode configuration by using Co_2P / Co_2P and CoP / CoP as anode / cathode in 1 M KOH at 65 ℃.

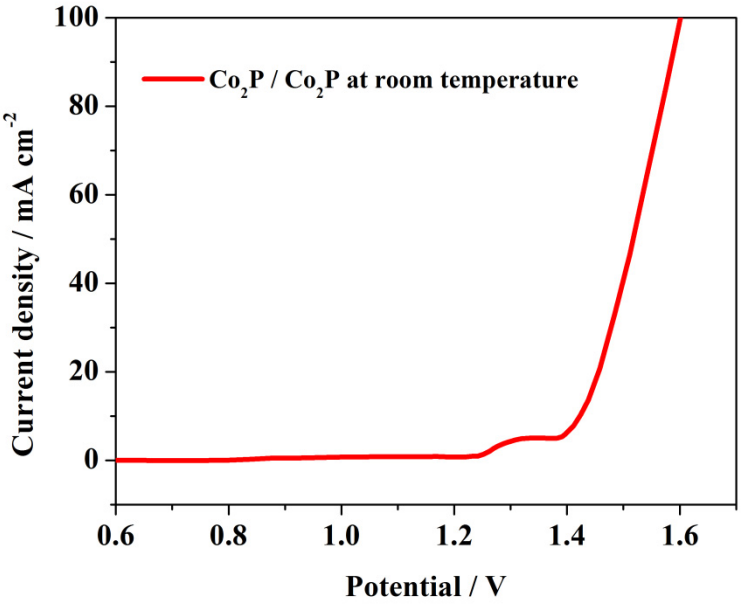

Fig. S17 Polarization curves of the two-electrode configuration by using Co_2P / Co_2P at room temperature.

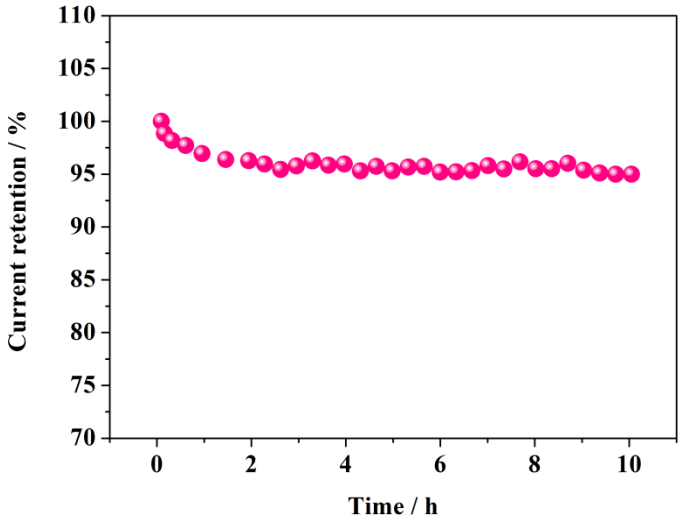

Fig. S18 The stability of the two-electrode configuration based on Co_2P NWs as both anode and cathode for alkaline water splitting. Cell voltage : 1.45 V, temperature: 65 ℃, electrolyte : 1 M KOH.

Additional characterizations of the catalyst after OER:

Fig. S19 XPS survey spectra and **Table S4** corresponding elemental contents on the near-surface region (< 10 nm depth) of the anode (Co_2P) before and after CV scanning.

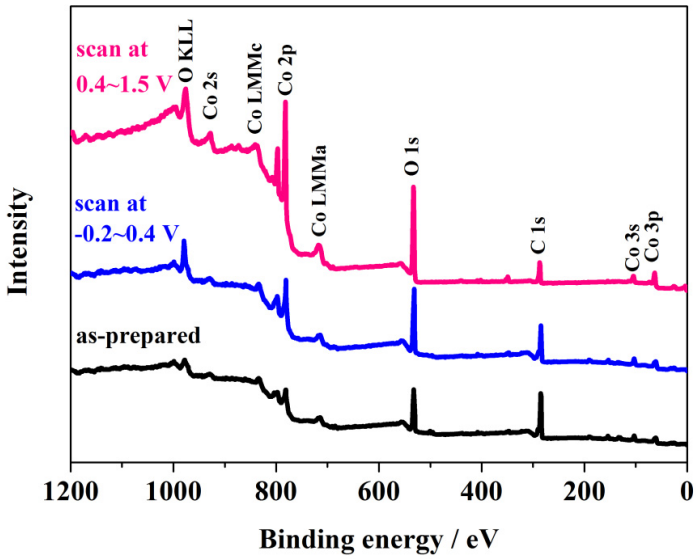

as-prepared:

element	Atom Conc.%	Mass Conc.%
Co	27.9	54.3
P	15.6	15.9
O	56.5	29.8

scan at -0.2 ~ 0.4 V:

element	Atom Conc.%	Mass Conc.%
Co	18.0	43.3
P	5.3	6.7
O	76.7	50.0

scan at 0.4 ~ 1.5 V:

element	Atom Conc.%	Mass Conc.%
Co	8.02	24.09
P	1.37	2.08
O	90.61	73.83

The increase of oxygen reveals the $Co(OH)_2$ and CoO_x generated on the surface at the different potential window.

Fig. S20 HRTEM images of the Co_2P nanowire after electrocatalysis (OER) in 1 M KOH.

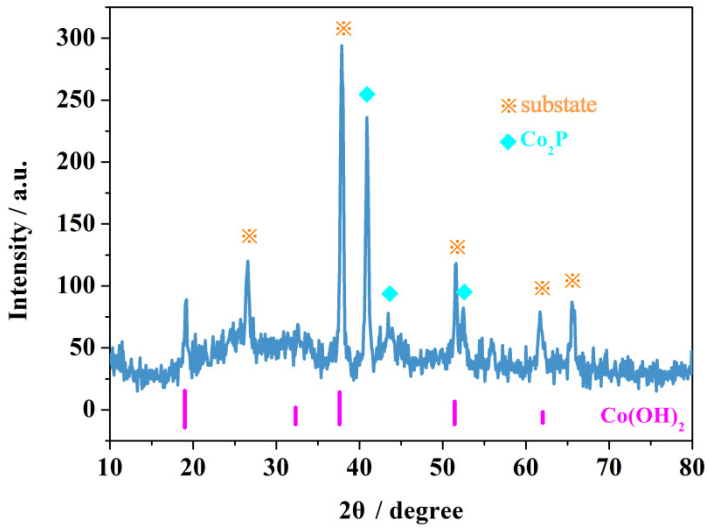

Fig. S20 XRD pattern of the Co_2P after the CV scanning between -0.2 V and 0.4 V for 30 cycles; the ball-stick model shows the schematic structure of the cobalt oxo/hydroxide unit connecting with a phosphate group.

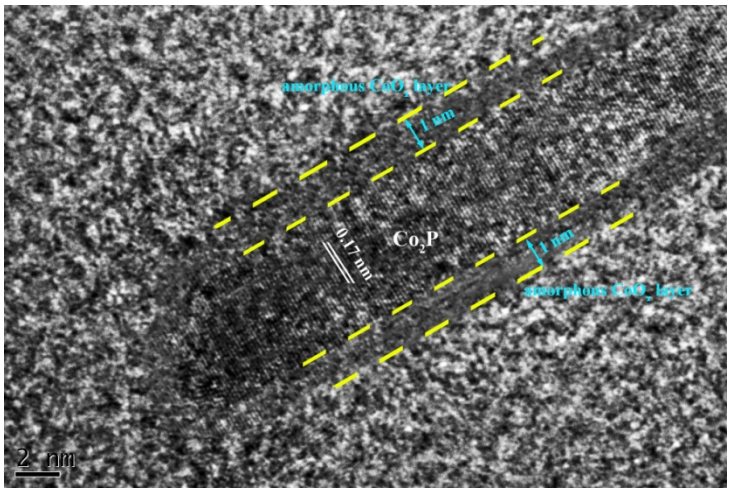

Fig. S21 HRTEM images of the Co_2P nanowire after electrocatalysis (OER) in 1 M KOH.

Table S5 Comparisons of the various HER catalysts in acidic electrolyte according to the reports and this paper.

catalyst	**η_{onset} (mV)**	**$\eta_{j=10\ mA\ cm-2}$ (mV)**	**$\eta_{j=20\ mA\ cm-2}$ (mV)**	**Tafel slope (mV dec^{-1})**	**substrate**	**catalyst laoding (mg cm^{-2})**	**reference**
Ni_2P	-	117	130	46	Ti foil	1	[8]
CoP	38	67	100	51	carbon cloth	0.92	[9]
MoP	50	135	167	54	GCE	0.86	[10]
Cu_3P	62	143	-	67	Cu foam	15.2	[11]
MoS_2/rGO	100	154	176	41	GCE	0.28	[12]
$CoSe_2$		231	-	42	GCE	0.037	[13]
Fe-WCN	100	220	-	47	GCE	0.4	[14]
Co_9S_8 /MoS_2	64	190	-	110	carbon nanofiber	0.212	[15]
CoP NWs	30	89	113	41	GCE	0.17	this work
Co_2P NWs	33	95	120	45	GCE	0.17	this work

Table S6 Comparisons of the various OER catalysts in alkaline electrolyte according to the reports and this paper.

catalyst	electrolyte	$\eta_{j=10\ mA\ cm-2}$ (V)	$\eta_{j=20\ mA\ cm-2}$ (V)	Tafel slope (mV dec^{-1})	substrate	catalyst loading (mg cm^{-2})	reference
Ni_2P	1 M KOH	290	310	59	GCE	0.14	[16]
CoP/C	0.1 M KOH	360	390	66	GCE	0.4	[17]
Fe-doped NiO	1M KOH	290	320	54	quartz crystal microbalance electrode	0.0225	[18]
$CoSe_2$	0.1 M KOH	320	360	44	GCE	0.142	[19]
reduced Co_3O_4	1 M KOH	410	450	72	GCE	0.136	[20]
NiFe LDH/NGF	0.1 M KOH	190	-	110	carbon nanofiber	0.25	[21]
CoP NWs	1 M KOH	320	360	64	GCE	0.17	this work
Co_2P NWs	1 M KOH	260	290	52	GCE	0.17	this work

Table S7 Comparisons of the two-electrode configuration performance according to the reports and this paper.

electrode	electrolyte	$U_{j=10\ mA\ cm-2}$ (V)	$U_{j=100\ mA\ cm-2}$ (V)	temperature (℃)	substrate	reference
Ni_2P/ Ni_2P NPs	1 M KOH	1.64	-	R.T.[a]	Ni foam	[16]
NiO-Ni	1 M KOH	1.43	1.57	R.T.	Ni foam	[22]
CNT/NiFe LDH		1.40	1.45	60		
NiSe/NiSe NWs	1 M KOH	1.63	-	R.T.	Ni foam	[23]
CoP/CoP nanorods	1 M KOH	1.62	-	R.T.	Ni foam	[24]
Co-P/Co-P film	1 M KOH	1.64	1.75	R.T.	Cu foil	[25]
Co_2P / Co_2P NWs	1 M KOH	1.44 1.38	1.60 1.46	R.T. 60	Ni foam	this work

[a] R.T.: room temperature

References:

1. A. E. Henkes and R. E. Schaak, *Chem. Mater.*, 2007, **19**, 4234-4242.
2. S. Y. Zhang, E. Y. Ye, S. H. Liu, S. H. Lim, S. Y. Tee, Z. L. Dong and M. Y. Han, *Adv. Mater.*, 2012, **24**, 4369-4375.
3. J. F. Callejas, C. G. Read, E. J. Popczun, J. M. McEnaney and R. E. Schaak, *Chem. Mater.*, 2015, **27**, 3769-3774.
4. S. J. Clark, M. D. Segall, C. J. Pickard, P. J. Hasnip, M. J. Probert, K. Refson and M. C. Payne., *Z. Kristallogr.*, 2005, **220**, 567-570.
5. A. P. Grosvenor, S. D. Wik, R. G. Cavell and A. Mar, *Inorg. Chem.*, 2005, **44**, 8988-8998.
6. D. Yang, J. X. Zhu, X. H. Rui, H. T. Tan, R. Cai, H. E. Hoster, D. Y. W. Yu, H. H. Hng and Q. Y. Yan, *ACS Appl. Mat. Interfaces*, 2013, **5**, 1093-1099.
7. W. X. Peng, L. F. Jiao, Q. N. Huan, L. Li, J. Q. Yang, Q. Q. Zhao, Q. H. Wang, H. M. Du, G. Liu, Y. C. Si, Y. J. Wang and H. T. Yuan, *J. Alloys Compd.*, 2012, **511**, 198-201.
8. E. J. Popczun, J. R. McKone, C. G. Read, A. J. Biacchi, A. M. Wiltrout, N. S. Lewis and R. E. Schaak, *J. Am. Chem. Soc.*, 2013, **135**, 9267-9270.
9. J. Q. Tian, Q. Liu, A. M. Asiri and X. P. Sun, *J. Am. Chem. Soc.*, 2014, **136**, 7587-7590.
10. P. Xiao, M. A. Sk, L. Thia, X. M. Ge, R. J. Lim, J. Y. Wang, K. H. Lim and X. Wang, *Energy Environ. Sci.*, 2014, **7**, 2624-2629.
11. J. Q. Tian, Q. Liu, N. Y. Cheng, A. M. Asiri and X. P. Sun, *Angew. Chem. Int. Ed.*, 2014, **53**, 9577-9581.
12. Y. Li, H. Wang, L. Xie, Y. Liang, G. Hong and H. Dai, *J. Am. Chem. Soc.*, 2011, **133**, 7296-7299.
13. D. Kong, J. J. Cha, H. Wang, H. R. Lee and Y. Cui, *Energy Environ. Sci.*, 2013, **6**, 3553-3558.

14. Y. Zhao, K. Kamiya, K. Hashimoto and S. Nakanishi, *Angew. Chem. Int. Ed.*, 2013, **52**, 13638-13641.
15. H. Zhu, J. Zhang, R. Yanzhang, M. Du, Q. Wang, G. Gao, J. Wu, G. Wu, M. Zhang, B. Liu, J. Yao and X. Zhang, *Adv. Mater.*, 2015, **27**, 4752-4759.
16. L. A. Stern, L. G. Feng, F. Song and X. L. Hu, *Energy Environ. Sci.*, 2015, **8**, 2347-2351.
17. J. Ryu, N. Jung, J. H. Jang, H.-J. Kim and S. J. Yoo, *ACS Catal.*, 2015, **5**, 4066-4074.
18. K. Fominykh, P. Chernev, I. Zaharieva, J. Sicklinger, G. Stefanic, M. Doblinger, A. Muller, A. Pokharel, S. Bocklein, C. Scheu, T. Bein and D. Fattakhova-Rohlfing, *ACS Nano*, 2015, **9**, 5180-5188.
19. Y. W. Liu, H. Cheng, M. J. Lyu, S. J. Fan, Q. H. Liu, W. S. Zhang, Y. D. Zhi, C. M. Wang, C. Xiao, S. Q. Wei, B. J. Ye and Y. Xie, *J. Am. Chem. Soc.*, 2014, **136**, 15670-15675.
20. Y. C. Wang, T. Zhou, K. Jiang, P. M. Da, Z. Peng, J. Tang, B. A. Kong, W. B. Cai, Z. Q. Yang and G. F. Zheng, *Adv. Energy Mater.*, 2014, **4**, 1400696.
21. C. Tang, H. S. Wang, H. F. Wang, Q. Zhang, G. L. Tian, J. Q. Nie and F. Wei, *Adv. Mater.*, 2015, **27**, 4516-4522.
22. M. Gong, W. Zhou, M. C. Tsai, J. G. Zhou, M. Y. Guan, M. C. Lin, B. Zhang, Y. F. Hu, D. Y. Wang, J. Yang, S. J. Pennycook, B. J. Hwang and H. J. Dai, *Nat. Commun.*, 2014, **5**, 4695-4700.
23. C. Tang, N. Y. Cheng, Z. H. Pu, W. Xing and X. P. Sun, *Angew. Chem. Int. Ed.*, 2015, **54**, 9351-9355.
24. Y.-P. Zhu, Y.-P. Liu, T.-Z. Ren and Z.-Y. Yuan, *Adv. Funct. Mater.*, 2015, 10.1002/adfm.201503666.
25. N. Jiang, B. You, M. L. Sheng and Y. J. Sun, *Angew. Chem. Int. Ed.*, 2015, **54**, 6251-6254.